Highly Selective Optical Detection of Fe^{3+} ions in Aqueous Solution using Label-Free Silicon Nanocrystals

*Keith Linehan, Darragh Carolan and Hugh Doyle**

Dr. K. Linehan, Dr. H. Doyle
Tyndall National Institute, University College Cork, Lee Maltings, Cork, Ireland.
E-mail: hughjdoyle@gmail.com

Dr. D. Carolan
Nanotechnology & Integrated Bio-Engineering Centre, University of Ulster, Shore Road, Newtownabbey, Northern Ireland.

Keywords: nanocrystal, sensor, optical detection, iron

High brightness amine-terminated silicon nanocrystals (Si NCs) have been utilized in a simple and rapid assay for the highly selective and sensitive detection of Fe^{3+} *via* quenching of their strong blue luminescence, without the need for analyte-specific labelling groups. Sensitive detection of Fe^{3+} was successfully demonstrated, with a linear relationship observed between luminescence quenching and Fe^{3+} concentration from 5 - 900 μM and a limit of detection of 1.3 μM. The Si NCs show excellent selectivity toward Fe^{3+} ions, with no quenching of the luminescence signal induced by the presence of Fe^{2+} ions, allowing for solution phase discrimination between the ionic species in different charge states.

1. Introduction

Semiconductor nanocrystals (NCs) have received considerable interest in the last 30 years due to their tunable optoelectronic properties, leading to applications ranging from displays and photovoltaics to luminescent labels for in-vivo imaging.[1] Their chemical robustness and photostability have made NCs especially attractive as luminescent probes for chemical and biological sensing, opening up new strategies for simple, sensitive, on-site analysis of specific targets.[2] Due to public concerns regarding the biological impact of transition and heavy metal ions, there is a continuing demand for the development of sensitive assays that are operable in living systems and the environment.[3]

For semiconductor nanocrystals to be utilized in optically addressed sensing applications, they must be sufficiently chemically robust to withstand challenging sample conditions, show minimal perturbation to the system probed (*i.e.* low or no toxicity) and produce intense but switchable responses to incident light, yielding a strong signal change upon analyte interaction.[2, 4] Despite their high quantum yields, resistance to photobleaching and size tunable emission profiles, concerns have been raised over the heavy metal (Cd, Pb, Hg) content of the widely used II-VI nanomaterials, which can be toxic even at relatively low concentrations.[5] In addition, the higher disposal costs for heavy metal containing waste and legislation enacted in several jurisdictions severely restrict their use in industrial and consumer applications.[6] These issues have driven research into the development of heavy metal free alternatives, such as group IV materials (Si, Ge),[7] ternary I-III-VI alloys (CIGS, CZTS)[8] and metal-organic frameworks (MOFs)[9] that would exhibit similar desirable photophysical properties but do not represent a health or environmental hazard.

Yi *et al.* reported on the use of Si NCs as an environmentally friendly probe for glucose detection; the NC luminescence was quenched by H_2O_2 produced from the oxidation of glucose

by glucose oxidase.[10] The Zhang group later demonstrated the detection of Cu^{2+} and pesticides in nanomolar quantities using this approach.[11] A colorimetric assay for glucose was also realized using the Si NCs as a peroxidase mimic to catalyze the oxidation of 3,3',5,5'-tetramethylbenzidine by H_2O_2 to produce a measurable color change.[12] The Chen group reported dopamine detection with a linear response range from 5 nM to 10 μM by luminescence quenching in water-dispersed Si NCs.[13] Zhang and Yu designed a recyclable strategy for the rapid detection of Hg^{2+} in aqueous solution with a detection range of 50 nM to 1 μM.[14] Due to the strong interaction of Hg^{2+} with thiol groups, the luminescence could be fully recovered by introduction of biothiols such as cysteine and glutathione. More recently, Campos *et al.* reported a luminescent sensor for Cr^{4+} based on Si NCs functionalized with hydroxyl PAMAM dendrimers.[15] Ban *et al.* reported TNT detection in aqueous solutions over 5 – 500 nM *via* the formation of a (TNT-amine) Meisenheimer complex at the Si NC surface.[16] Veinot and co-workers have demonstrated the detection of high energy compounds including 2,4,6-trinitrotoluene (TNT), 1,3,5-trinitroperhydro-1,3,5-triazine (RDX) and pentaerythritol tetranitrate (PETN) in the solid, solution and vapor phases.[17]

Iron is a biologically essential metal that is a component of several metalloproteins and plays a crucial role in vital biochemical activities,[18] while iron levels are important criteria in the evaluation of drinking water quality.[19] In this paper, we report on the synthesis and characterization of water-dispersed Si NCs as a simple and rapid sensing platform for the detection of ferric (Fe^{3+}) ions. Quenching of the Si NC luminescence is the transduction method used for selective detection of Fe^{3+} in aqueous solution. The linear response range and limit of detection were investigated by photoluminescence spectroscopy, while the mechanism was confirmed by time-resolved luminescence measurements.

2. Results and discussion

2.1. Si NC Characterization

TEM imaging of the Si NCs showed them to be non-uniform, with diameters between 3 – 8 nm, with some evidence of shape anisotropy, see **Figure 1**(a). Figure 1(b) shows a histogram of 200 NC diameters measured at random locations across the grid. Fitting the data to a Gaussian distribution yields an average NC diameter of 5.4 nm, with a standard deviation of 1.5 nm. While the internal atomic arrangement of Si NCs in this size range would be expected to be transitioning between that of a cluster and the bulk, high resolution TEM (HR-TEM) imaging, see Figure 1(c), show that the NCs possess a highly crystalline core with a relaxed surface layer. The less crystalline arrangement of the NC surface is probably due to the combined effects of chemical functionalization and partial surface oxidation, as confirmed by FTIR (see below). The selected area electron diffraction (SAED) pattern shows reflections at *d* spacings of 1.9, 1.6, 1.3 and 1.2 Å, consistent with the (220), (311), (400) and (331) reflections reported for the Si (*Fd3m*) lattice,[20] see Figure 1(d). It was not possible to confirm the phase purity of the Si NCs by powder X-ray diffraction, due to the small quantity of NCs prepared and the relatively low X-ray scattering factor of silicon: similar difficulties have been encountered in the structural characterization of Ge NCs prepared *via* this synthetic approach.[21]

Figure 2 shows the FTIR spectrum of the amine-terminated Si NCs. The peaks at 3695 and 3623 cm^{-1} are assigned to N–H stretching of the amine, while the features observed at 1685 and 1604 cm^{-1} are attributed to N−H scissoring and bending modes. The Si NCs exhibit clear C-H stretching signals, with symmetric CH_2, asymmetric CH_2, and the asymmetric C-CH_3 stretching modes at 2977, 2893 and 2852 cm^{-1}, respectively. The peak at 1386 cm^{-1} is attributed to C-H bending modes. The peak at 1261 cm^{-1} is assigned to vibrational scissoring of the Si−C bond formed by covalent binding of the allylamine ligand to the NC surface.[22] The features between 1100 – 1000 $cm^{-1}$are attributed to the vibrational stretching of SiO_x species, indicative

of partial surface oxidation. The absence of bending band at *ca.* 1430 cm^{-1}, assigned to the quaternary ammonium ion (NR_4^+), indicates that the surfactant was fully removed during the post-synthetic purification.[23]

The surface chemistry was further characterized by XPS spectroscopy; see **Figure 3**. The Si2p spectra shown in Figure 3(a) shows a weak signal centered at 102.8 eV, attributed to the presence of Si−O_x species at the NC surface. The C1s spectrum (see Figure 3(b)) is well fitted with two main peaks at 284.8 and 286.15 eV, assigned to C−Si and C-C/C-H bonds in the covalently attached amine ligands, with a minor peak at 288.5 eV attributed to surface adsorbed CO_x species. The O1s spectrum in Figure 3(c) has one peak centered at 532.2 eV, assigned to SiO_x groups at the nanocrystal surface. The N1s spectrum, see Figure 3(d), is well fitted with a four-peak fit, with the main peak at 399.0 eV due to C-N bonds,[24] and three minor peaks at 401.53, 403.56 and 405.2 eV attributed to N-H bonds and trace amounts of other species such as N-C=O. The full survey photoelectron spectrum, see **Figure S1** of the Supporting Information, shows the presence of additional peaks at 197.1 eV and 67.2 eV, which are attributed to presence of residual Cl and Br from the synthesis.

Optical characterization of the Si NCs showed a strong absorbance in the UV region, with a shoulder at *ca*. 320 nm (3.85 eV), and an onset of absorbance near 400 nm (3.1 eV), see **Figure 4**. These quantum confinement effects have been observed in literature reports for similarly sized Si NCs, and are attributed to direct electronic transitions from the valence band at Γ_{25} to the split conduction bands at Γ_{15}.[25] PL spectra of the Si NCs exhibit a violet/blue luminescence, with the wavelength position of the luminescence maximum red-shifting from 415 nm to 555 nm as the excitation wavelength is increased from 320 nm to 520nm, see also **Figure S2** of the Supporting Information. This excitation wavelength dependence been reported previously for Si NCs with covalently bound ligands, and shown to be due to the involvement of different

surface species in the luminescence process, rather than NC size polydispersity.[25b, 25d, 26] PL spectra recorded at different excitation wavelengths shows a maximum luminescence intensity under illumination at 360 nm (see Figure S2), in good agreement with the photoluminescence excitation (PLE) spectrum (see Figure 4), which shows a narrow peak centered at *ca.* 355 nm (3.5 eV), confirming that the optimal excitation wavelength lies well above the band gap energy of the Si NCs.

The photophysical properties observed closely match our previous reports for Si NCs,[20, 27] implying that the same luminescence mechanism may be responsible: UV illumination above the band gap energy results in efficient exciton generation within the crystalline core, followed by radiationless transfer and radiative recombination at states near the NC surface. This agrees with literature reports that emphasize the importance of surface species in the radiative recombination mechanisms of Group IV NCs.[7a, 7c, 7e, 25d, 26]The violet/blue luminescence and nanosecond lifetimes observed (see below), are consistent with a surface state based luminescence mechanism, rather than exciton recombination within the crystalline core, which is associated with orange/red luminescence and microsecond lifetimes.[28] It is noted that the Si NCs exhibit excellent photostability, with the luminescence intensity decreasing less than 3% after continuous illumination for 5 hours, see **Figure S3** of the Supporting Information.

2.2. Quenching of Nanocrystal Luminescence

PL spectra of the Si NCs recorded at increasing Fe^{3+} concentrations (0 - 900 μM) are shown in **Figure 5**(a). Increasing the Fe^{3+} concentration resulted in a monotonic decrease in the PL intensity, with no change in the wavelength position of the luminescence maximum, nor the full width at half maximum, indicating that that no new emissive species were formed following exposure to ferric ions. Figure 5(b) shows a Stern-Volmer plot of I_0/I versus Fe^{3+} ion concentration, where I_0 and I are the luminescence intensities before and after addition of the

analyte ions, respectively. For Fe^{3+}, the experimental data shows the linear relationship predicted by the Stern-Volmer equation, $I_o/I = 1 + K_{SV}[Q]$, where K_{SV} is the Stern-Volmer constant and $[Q]$ is the quencher concentration. The lack of curvature in the plot indicates that only one quenching mechanism is present.[29] To quantify the linear response range and limit of detection, the decrease in luminescence intensity with increasing Fe^{3+} concentration was fitted with a least squares linear model. The fitting yielded a Stern-Volmer constant, K_{SV}, of 1.4 x 10^3 ± 6.8 x 10^1 M^{-1} with a correlation coefficient, R^2 = 0.98. The limit of detection (LOD) was determined to be 1.3 μM, from $LOD = 3\sigma_{blank}/K_{SV}$, where σ_{blank} is the standard deviation of the blank measurements recorded in the absence of the analyte.[30] In contrast to the results obtained for ferric ions, the presence of Fe^{2+} ions does not result in any decrease in luminescence intensity, with I_o/I remaining constant at all Fe^{2+} concentrations investigated.

2.3. Luminescence Quenching Mechanism

As the NCs emit at lower energies (2.2 – 3.0 eV) than the absorbance range of the analyte ions (ca. 3.5 - 5.0 eV),[31] it is unlikely that the luminescence decrease is due to resonance energy transfer or an electron exchange (Dexter) interaction, as both mechanisms depend on spectral overlap between the donor and acceptor.[29] Luminescence quenching *via* intersystem crossing, due to dissolved oxygen in the NC dispersions, would not account for the linear relationship between I_0/I and Fe^{3+} concentration, nor the discrimination between Fe^{2+} and Fe^{3+} ions. As a result, the only plausible mechanism for the luminescence quenching is photoinduced electron transfer (PET) between the NC surface states involved in luminescence and the analyte ions. Quenching may proceed *via* a dynamic or static process: dynamic (or collisional) quenching occurs when the analyte interacts directly with the excited state, resulting in a change in the luminescence lifetime. In contrast, static quenching results from the formation of a non-emissive ground state complex between the analyte and the luminophore: since any residual emission originates from non-complexed luminophores, the lifetimes are unaffected.[29]

Time-resolved photoluminescence spectroscopy measurements were performed on Si NCs before and after exposure to Fe^{3+} to confirm the underlying quenching mechanism, see **Figure 6**. Nanosecond intensity transients of Si NC before exposure were well fitted to the sum of three weighted exponentials, with an amplitude-weighted average lifetime $\langle\tau\rangle_a = \sum a_i\tau_i / \sum a_i$)[32] of 1.8 ns;[32] see **Table S1** of the Supporting Information for fitted time constants and fractional amplitudes. Transients recorded after exposure to Fe^{3+} (50 μM) yielded an average lifetime of 1.9 ns, in close agreement with that recorded in the absence of the analyte ions. The similarity of luminescence lifetimes supports the assignment of a static quenching mechanism, which is consistent with the absence of changes to the PL spectra recorded at different ferric ion concentrations. Time resolved measurements on Si NCs in the presence of Fe^{2+} ions showed a similar average lifetime, see Figure S4 and Table S1 of the Supporting Information. The close agreement in the excited state lifetimes recorded before and after addition of analyte ions indicates that the luminescence quenching of the Si NCs proceeds *via* a static mechanism, where the Fe^{3+} ions diffuse to the NC surface to form a complex that provides increased numbers of non-radiative recombination pathways.

This finding is not surprising, given the nanosecond excited state lifetimes and the micromolar concentrations involved. If the quenching did proceed *via* a dynamic mechanism, the analyte ions would have to diffuse to the NC surface from solution during the excited state lifetime, *i.e.* before radiative recombination can occur. The root-mean-square distance (d_{rms}) that an ion can diffuse is given by $d_{rms} = \sqrt{2D\tau}$, where D is the diffusion coefficient and τ is the lifetime.[29] As the diffusion constant of a Fe^{3+} ion in water at 25 ºC is 6.04 x 10^{-10} m^2s^{-1},[33] and the Si NC luminescent lifetime is 1.9 ns, the ferric ions must be within 1.5 nm of the NC surface for dynamic quenching to occur. This, in turn, defines a spherical "shell" with a 1.5 nm thickness surrounding the NC where the ions must be present for dynamic quenching to take place. The volume of this interaction region is calculated to be 2.3 x 10^{-25} m^3, see the Supporting

Information for further details. However, at K_{sv}^{-1} (7.1 x 10^{-4} M), the concentration at which I_0/I = 2 (*i.e.* 50% of the luminescence is quenched), there is one analyte ion every 2.3 x 10^{-24} m^3, assuming a homogeneous solution. This implies that only one in every 10 NCs would have a Fe^{3+} ion close enough in solution to diffuse to the surface within the excited state lifetime. At the limit of detection for Fe^{3+} ions, 1.3 μM, the probability drops to 0.02%. Consequently, is highly unlikely that the luminescence response shown in Figure 5 can be the result of a dynamic quenching mechanism.

Further insight into the underlying mechanism may be obtained from the bimolecular quenching constant, $k_q = K_{SV}/\langle\tau\rangle_i$,[29] where $\langle\tau\rangle_i = \sum a_i\tau_i^2/\sum a_i\tau_i$ is the intensity-weighted average lifetime.[32] This rate constant relates to the encounter frequency and subsequent quenching efficiency between a luminophore and a quencher, with values near 1 x 10^{10} $M^{-1}s^{-1}$ considered the upper limit for diffusion controlled quenching in aqueous solution.[29] Lower k_q values are usually the result of steric shielding or low quenching efficiencies, while higher values indicate some type of binding interaction. The value of k_q found in this study is 2.2 x 10^{11} $M^{-1}s^{-1}$, over an order of magnitude above the diffusion limit, providing further support that the Si NC luminescence quenching occurs *via* a static binding mechanism.

2.4. Discrimination between Ferrous and Ferric Ions

The different responses exhibited by the Si NCs to the presence of ferrous (Fe^{2+}) and ferric (Fe^{3+}) ions may be explained in terms of the thermodynamics of the quenching interaction. In PET, a complex is formed between an electron donor (D) and an acceptor (A); upon excitation, the donor transfers an electron to the acceptor, forming the charge transfer complex $[D^+A^-]^*$.[29] For oxidative quenching (where the luminophore is the electron donor) the overall free energy change (ΔG) for electron transfer is given by:[34]

$$\Delta G = nF[E(NC^+/NC) - E_{00}(NC^*/NC) - E(A/A^-)] + w \quad (1)$$

where n is the number of electrons involved in the reaction, F is the Faraday constant, $E(NC^+/NC)$ and $E(A/A^-)$ are the reduction potentials of the Si NCs and analyte ions (electron acceptors), $E_{00}(NC^*/NC)$ is the one electron potential corresponding to the optical band gap of the Si NCs, while w accounts for the Coulombic interaction between ion pair after electron transfer. For the results reported above, both $E(NC^+/NC)$ and $E_{00}(NC^*/NC)$ remain constant, so the differences in luminescence quenching observed are due to the reduction potentials of the analyte ions. The electrostatic term (w) is relatively small and may be neglected when comparing a series of homogeneous electron transfer reactions in the same solvent between the same electron donor and a series of structurally related acceptors. The standard reduction potentials for $Fe^{3+/}Fe^{2+}$ is +0.771 V *vs.* SHE,[35] resulting in a net negative contribution to the free energy of the reaction, whereas the reduction potential for Fe^{2+}/Fe^{+} is -0.447 V *vs.* SHE,[35] a net positive contribution. As a result, luminescence quenching by Fe^{3+} ions is thermodynamically favored compared to quenching by Fe^{2+} ions.

2.5. Effect of Interferents

Since PET typically occurs over separations of less than a nanometer, it can be sensitive to molecular effects, such as chemical bonding and Coulombic interactions, that affect the contact between the electron donor and acceptor. To investigate whether the luminescence quenching was affected by the chemical identity of the analyte ions, the Si NCs were exposed to several first row transition metal ions (Mn^{2+}, Co^{2+}, Ni^{2+}, Cu^{2+}, and Zn^{2+}), as well as some heavy metal ions of known toxicity (Cd^{2+}, Hg^{2+} and Pb^{2+}). **Figure 7** shows the relative luminescence intensity (I/I_0) of the Si NCs following exposure to 50 μM of the metal ions. As may be seen from the data, most of the metal ions examined elicited little or no response, with only Ni^{2+} ions showing a modest response (6% quenching). However, both Cu^{2+} and Hg^{2+} would be expected

to cause significant decrease in the luminescence intensity, while Ni^{2+} should only show a weak quenching effect, see **Table S2** of the Supporting Information for the reduction potentials of the analyte ions used.[35]

It is evident that the efficiency and extent of the luminescence quenching can be as dependent on the chemical identity of the quencher as it is on the energetics of the PET interaction. This, in turn, requires that the different responses observed be considered in terms of the relative binding affinity of the analyte ions to chemical species present at the NC surface. While the allylamine ligands covalently bound at the NC surface provide NH_2 binding sites, FTIR and XPS measurements (see Figure 2 and Figure 3) also reveal the presence of Si-O_x species. While oxygenic species (hard Lewis bases) are known to readily bind hard acids such as Ni^{2+}, softer acids such as Cu^{2+} and Hg^{2+} show an affinity for nitrogen containing functional groups.[36] At the pH used in these experiments (*ca*. 5.5 – 6.5 due to dissolved atmospheric CO_2), the allylamine ligands (with a pK_a of 9.5) should be protonated to $-NH_3^+$, impeding their binding to positively charged ions. The higher acidity of Si-O_x species may allow them to bind Ni^{2+} ions from solution, resulting in the luminescence quenching observed. In other words, while PET by Ni^{2+} is less favorable energetically, the ions are able to approach close enough to the NC surface for PET to occur. It is difficult to assess whether it is the exergonicity of the electron transfer interaction or the binding affinity of NC surface species toward the analyte ions that most affects the luminescence quenching in Si NCs: it is likely that the responses shown in Figure 7 are determined by contributions from both influences.

3. Conclusion

The use of Si NCs as a simple and rapid sensing platform for the detection of ferric (Fe^{3+}) ions in aqueous solutions, without the need for analyte-specific labelling groups, has been demonstrated. A linear relationship between luminescence quenching and Fe^{3+} concentration

was observed from 5 - 900 μM, with a limit of detection of 1.3 μM. The Si NCs show excellent selectivity toward Fe^{3+} ions, with no quenching of the luminescence signal induced by the presence of Fe^{2+} ions, allowing for aqueous phase discrimination between iron ions in different charge states. The Si NCs did not exhibit a significant quenching response to the presence of other first row transition metal ions and were completely insensitive to heavy metal ions. The excellent photostability of the Si NCs, combined with high specificity toward Fe^{3+}, suggest that this optical sensing approach can be developed for future use in medical or environmental monitoring applications.

4. Experimental Section

Nanocrystal synthesis The synthesis of water dispersible Si NCs was adapted from our previously reported methods.[20, 27] All reagents and solvents were reagent grade or higher and used as received. All glassware used was cleaned by thoroughly soaking in a base bath overnight, followed by immersion in piranha solution (3:1 concentrated sulfuric acid: 30% hydrogen peroxide) for 20 min. In an inert atmosphere glove-box, tetraoctylammonium bromide (3 g, 5.46 mmol, TOAB) was dissolved in anhydrous toluene (100 mL). $SiCl_4$ (1.0 mL, 8.7 mmol) was then added to the solution and left to stir for 30 min. Silicon nanocrystals were formed by the dropwise addition of lithium tri-*sec*-butylborohydride hydride (6 mL, 1 M) in THF over a period of 2 min. The solution was then left to react for 2.5 h. The excess reducing agent was then quenched with the addition of methanol (60 mL), upon which the dispersion became transparent

The Si NC surfaces were functionalized *via* the addition of H_2PtCl_6 in isopropyl alcohol (0.5 mL, 0.1 M) as a catalyst, followed by allylamine (4.5 mL). After stirring for 2.5 h, the amine-terminated Si NCs were removed from the box and the organic solvent removed by rotary

evaporation. The resulting dry powder was then redispersed in deionized (DI) water (20 mL, 18.2 MΩcm) and sonicated for 30 min. The solution was centrifuged at 10,000 rpm for 10 minutes and filtered twice using PVDF membrane filters (MILLEX-HV, Millipore, 0.45 µm) to remove the surfactant before loading onto a chromatography column. Sephadex gel LH-20 was used as the stationary phase and DI water as the eluent. Fractions were collected at a flow rate of one drop every 5 s. A hand held UV lamp (365 nm) was used to check each fraction for Si NCs luminescence. The fractions were then combined and concentrated down to *ca.* 20 mL.

Structural characterization Transmission electron microscopy (TEM) images and selective area electron diffraction patterns (SAED) were acquired using a high-resolution JEOL 2100 electron microscope, equipped with a LaB_6 electron source and Gatan DualVision 600 Charge-Coupled Device (CCD), operating at an accelerating voltage of 200 keV. Samples were prepared by depositing 300 µL of the Si NC dispersion onto a holey carbon coated TEM grid (400-mesh, #S147-3H, Agar Scientific), which was left to evaporate to dryness under ambient conditions. X-ray photoelectron spectroscopy (XPS) measurements of the Si NCs were carried out using a Kratos Ultra DLD photoelectron spectrometer. The narrow scan spectra were obtained under high vacuum conditions by using a monochromatic Al Kα x-ray radiation at 15 kV and 10 mA with an analyzer pass energy of 20 eV. Substrates were cleaned for 20 min in piranha solution, rinsed with water and dried with nitrogen. A few drops of the Si NC solution dissolved in chloroform were dropped on a clean gold surface substrate. All spectra were acquired at room temperature and binding energies were referenced to the Au $4f_{7/2}$ line. All spectra were corrected using a Shirley background.

Optical characterization FTIR spectra were recorded on a Perkin Elmer Two spectrometer. Spectra of Si NCs dispersed in chloroform were recorded in a liquid cell with CaF_2 plates. UV-Vis absorption spectra were recorded using a Shimadzu UV PC-2401 spectrophotometer

equipped with a 60 mm integrating sphere (ISR- 240A, Shimadzu). Spectra were recorded at room temperature using a quartz cuvette (1 cm) and corrected for the solvent absorption. Photoluminescence (PL) spectra were recorded using an Agilent Cary Eclipse spectrophotometer. Photostability measurements were recorded using an excitation wavelength of 360 nm and a 60 s integration time, and the resultant spectra integrated from 400 - 550 nm. Luminescence lifetime measurements were recorded on a scanning confocal fluorescence microscope (MicroTime 200, PicoQuant GmbH) equipped with a TimeHarp 200 TCSPC board. NC samples were excited using a 402 nm pulsed diode laser (10 MHz; 70 ps pulse duration, LDH-P-C-400) that was spectrally filtered using a 405 nm band-pass filter (Z405/10x, Chroma Technology Corp.). A 50X objective (0.5 NA; LM Plan FL, Olympus Corp.) was used for focusing the excitation light onto the NC dispersion and collecting the resultant fluorescence, which was directed onto an avalanche photodiode (APD; SPCM-AQR-14, Perkin-Elmer Inc.). Backscattered excitation light was blocked with a 410 nm long-pass filter placed in the collection path (3RD410LP, Omega Optical). The excitation power was adjusted to maintain a count rate of $< 10^4$ counts/s at the APD to preserve single photon counting statistics. All emission lifetimes were fitted with a weighted multi-exponential model on FluoFit 4.2 software (PicoQuant GmbH).

Photoluminescence quenching studies $Cd(ClO_4)_2 \cdot 6H_2O$ (99.999%), $CoCl_2$ (97%), $CuCl_2$ (97%), $FeCl_2$ (98%), $Fe(NO_3)_3 \cdot 9H_2O$ (99.99%), $HgCl_2$ (≥ 99.5%), $MnCl_2$ (98%), $NiCl_2$ (98%), $PbCl_2$ (98%) and $Zn(CH_3COO)_2 \cdot 2H_2O$ (99.999% trace metal basis) were purchased from Sigma Aldrich and used as received. All solutions and dilutions were prepared using DI water (18.2 MΩ cm). In a typical assay, 0.5 mL of the Si NC dispersion was added to 2.5 mL of a known concentration of each metal ion. Blank measurements were performed by adding 0.5 mL of the Si NC dispersion to 2.5 mL of DI water. To allow for complete diffusion and mixing of the Si NCs with the analyte ions, PL spectra were recorded every 2 minutes until the loss of

luminescence intensity was less than 1% between consecutive scans (see Figure S5 and S6 of the Supporting Information). The luminescence intensity (360 nm excitation) in the presence of the analyte was then determined from an average of four consecutive scans.

Supporting Information
Supporting Information is available from the Wiley Online Library or from the author.

Acknowledgements
The authors would like to thank Dr. Fathima Laffir at University of Limerick for performing the XPS measurements. This work was supported by the European Commission under the FP7 Projects HYSENS (grant agreement no. 263091), COMMONSENSE (grant agreement no. 261809) and SNAPSUN (grant agreement no. 246310), as well as the Irish Higher Education Authority under the PRTLI program (Cycle 3 “Nanoscience” and Cycle 4 “INSPIRE”.

Conflict of Interest
The authors declare no conflict of interest.

Received: ((will be filled in by the editorial staff))
Revised: ((will be filled in by the editorial staff))
Published online: ((will be filled in by the editorial staff))

References

[1] a) *Semiconductor Nanocrystal Quantum Dots: Synthesis, Assembly, Spectroscopy and Applications* (Ed: A. Rogach), Springer-Verlag, Wien, **2008**, p. 372; b) *Semiconductor and Metal Nanocrystals: Synthesis and Electronic and Optical Properties (Ed:* V. I. Klimov), Marcel Dekker, New York, **2004**; c) *Nanoparticles*, 2nd ed., (Ed: G. Schmid), Wiley-VCH, Weinheim, **2010**.

[2] a) Y. Lou, Y. Zhao, J. Chen, J.-J. Zhu, *J. Mater. Chem. C* **2014**, *2*, 595-613; b) P. Wu, T. Zhao, S. Wang, X. Hou, *Nanoscale* **2014**, *6*, 43-64.

[3] a) H. N. Kim, W. X. Ren, J. S. Kim, J. Yoon, *Chem. Soc. Rev.* **2012**, *41*, 3210-3244; b) D. T. Quang, J. S. Kim, *Chem. Rev.* **2010**, *110*, 6280-6301.

[4] a) R. Freeman, I. Willner, *Chem. Soc. Rev.* **2012**, *41*, 4067-4085; b) J. M. Costa-Fernández, R. Pereiro, A. Sanz-Medel, *Trends Analyt. Chem.* **2006**, *25*, 207-218.

[5] a) F. M. Winnik, D. Maysinger, *Acc. Chem. Res.* **2012**, *46*, 672-680; b) M. Bottrill, M. Green, *Chem. Commun.* **2011**, *47*, 7039-7050; c) N. Lewinski, V. Colvin, R. Drezek, *Small* **2008**, *4*, 26-49.

[6] a) European Parliament and Council, *Directive 2011/65/EU on the restriction of the use of certain hazardous substances in electrical and electronic equipment*, **2011**; b) *Measures for the Administration on Pollution Control of Electronic Information Products*, Ministry of Information Industry, China, **2007.**

[7] a) B. F. P. McVey, S. Prabakar, J. J. Gooding, R. D. Tilley, *ChemPlusChem* **2017**, *82*, 60-73; b) P. Reiss, M. Carrière, C. Lincheneau, L. Vaure, S. Tamang, *Chem. Rev.* **2016**, *116*, 10731-10819; c) K. Dohnalová, T. Gregorkiewicz, K. Kůsová, *J. Phys.: Condens. Matter* **2014**, *26*, 173201; d) S. Perraud, E. Quesnel, S. Parola, J. Barbé, V. Muffato, P. Faucherand, C. Morin, K. Jarolimek, R. A. C. M. M. Van Swaaij, M. Zeman, S. Richards, A. Kingsley, H. Doyle, K. Linehan, S. O'Brien, I. M. Povey, M. E. Pemble, L. Xie, K. Leifer, K. Makasheva, B. Despax, *Phys. Status Solidi A* **2013**, *210*, 649-657; e), *Silicon Nanocrystals* (Eds: L. Pavesi, R. Turan),

Wiley-VCH, Weinheim, **2010**; f) D. Carolan, *Prog. Mater. Sci.* **2017**, *90*, 128-158; g) D. D. Vaughn II, R. E. Schaak, *Chem. Soc. Rev.* **2013**, *42*, 2861-2879.

[8] a) C. Coughlan, M. Ibáñez, O. Dobrozhan, A. Singh, A. Cabot, K. M. Ryan, *Chem. Rev.* **2017**, *117*, 5865-6109; b) D. Aldakov, A. Lefrançois, P. Reiss, *J. Mater. Chem. C* **2013**, *1*, 3756-3776; c) A. Singh, S. Singh, S. Levcenko, T. Unold, F. Laffir, K. M. Ryan, *Angew. Chem. Int. Ed.* **2013**, *52*, 9120-9124; d) H. Zhong, Z. Bai, B. Zou, *J. Phys. Chem. Lett.* **2012**, *3*, 3167-3175.

[9] a) G.-W. Xu, Y.-P. Wu, W.-W. Dong, J. Zhao, X.-Q. Wu, D.-S. Li, Q. Zhang, *Small* **2017**, *13*, 1602996; b) Y.-P. Wu, G.-W. Xu, W.-W. Dong, J. Zhao, D.-S. Li, J. Zhang, X. Bu, *Inorg. Chem.* **2017**, *56*, 1402-1411; c) Z. Hu, B. J. Deibert, J. Li, *Chem. Soc. Rev.* **2014**, *43*, 5815-5840; d) L. E. Kreno, K. Leong, O. K. Farha, M. Allendorf, R. P. Van Duyne, J. T. Hupp, *Chem. Rev.* **2012**, *112*, 1105-1125; e) Y. Cui, Y. Yue, G. Qian, B. Chen, *Chem. Rev.* **2012**, *112*, 1126-1162.

[10] Y. Yi, J. Deng, Y. Zhang, H. Li, S. Yao, *Chem. Commun.* **2013**, *49*, 612-614.

[11] a) J. Zhao, J. Deng, Y. Yi, H. Li, Y. Zhang, S. Yao, *Talanta* **2014**, *125*, 372-377; b) Y. Yi, G. Zhu, C. Liu, Y. Huang, Y. Zhang, H. Li, J. Zhao, S. Yao, *Anal. Chem.* **2013**, *85*, 11464-11470.

[12] Q. Chen, M. Liu, J. Zhao, X. Peng, X. Chen, N. Mi, B. Yin, H. Li, Y. Zhang, S. Yao, *Chem. Commun.* **2014**, *50*, 6771-6774.

[13] X. Zhang, X. Chen, S. Kai, H.-Y. Wang, J. Yang, F.-G. Wu, Z. Chen, *Anal. Chem.* **2015**, *87*, 3360-3365.

[14] J. Zhang, S.-H. Yu, *Nanoscale* **2014**, *6*, 4096-4101.

[15] B. B. Campos, M. Algarra, B. Alonso, C. M. Casado, J. Jiménez-Jiménez, E. Rodríguez-Castellón, J. C. G. Esteves da Silva, *Talanta* **2015**, *144*, 862-867.

[16] R. Ban, F. Zheng, J. Zhang, *Anal. Methods* **2015**, *7*, 1732-1737.

[17] a) A. Nguyen, C. M. Gonzalez, R. Sinelnikov, W. Newman, S. Sun, R. Lockwood, J. G. C. Veinot, A. Meldrum, *Nanotechnology* **2016**, *27*, 105501; b) C. M. Gonzalez, M. Iqbal, M. Dasog, D. G. Piercey, R. Lockwood, T. M. Klapotke, J. G. C. Veinot, *Nanoscale* **2014**, *6*, 2608-2612.

[18] a) G. Papanikolaou, K. Pantopoulos, *Toxicol. Appl. Pharmacol.* **2005**, *202*, 199-211; b) P. Aisen, C. Enns, M. Wessling-Resnick, *Int. J. Biochem. Cell Biol.* **2001**, *33*, 940-959; c) N. C. Andrews, *N. Engl. J. Med.* **1999**, *341*, 1986-1995.

[19] World Health Organization, *Iron in Drinking-water: Background document for preparation of WHO Guidelines for drinking-water quality*, Geneva, **2003**.

[20] K. Linehan, H. Doyle, *Small* **2014**, *10*, 584-590.

[21] D. Carolan, H. Doyle, *Part. Part. Syst. Charact.* **2017**, *34*, 1600303.

[22] a) A. Shiohara, S. Hanada, S. Prabakar, K. Fujioka, T. H. Lim, K. Yamamoto, P. T. Northcote, R. D. Tilley, *J. Am. Chem. Soc.* **2010**, *132*, 248-253; b) J. H. Ahire, Q. Wang, P. R. Coxon, G. Malhotra, R. Brydson, R. Chen, Y. Chao, *ACS Appl. Mater. Interfaces* **2012**, *4*, 3285-3292.

[23] R. M. Silverstein, G. C. Bassler, T. C. Morrill, *Spectrometric Identification of Organic Compounds*, 5th ed., Wiley, New York, **1991**.

[24] A. Dementjev, A. De Graaf, M. Van de Sanden, K. Maslakov, A. Naumkin, A. Serov, *Diam. Relat. Mater.* **2000**, *9*, 1904-1907.

[25] a) J. P. Wilcoxon, G. A. Samara, *Appl. Phys. Lett.* **1999**, *74*, 3164-3166; b) A. Shiohara, S. Prabakar, A. Faramus, C. Y. Hsu, P. S. Lai, P. T. Northcote, R. D. Tilley, *Nanoscale* **2011**, *3*, 3364-3370; c) R. D. Tilley, J. H. Warner, K. Yamamoto, I. Matsui, H. Fujimori, *Chem. Commun.* **2005**, 1833-1835; d) J. H. Warner, H. Rubinsztein-Dunlop, R. D. Tilley, *J. Phys. Chem. B* **2005**, *109*, 19064-19067; e) J. H. Warner, A. Hoshino, K. Yamamoto, R. D. Tilley, *Angew. Chem. Int. Ed. Engl.* **2005**, *44*, 4550-4554.

[26] X. Cheng, S. B. Lowe, S. Ciampi, A. Magenau, K. Gaus, P. J. Reece, J. J. Gooding, *Langmuir* **2014**, *30*, 5209-5216.

[27] K. Linehan, H. Doyle, *Mater. Res. Soc. Symp. Proc.* **2013**, *1546*, mrss13-1546-l1506-1548.

[28] a) M. Dasog, K. Bader, J. G. C. Veinot, *Chem. Mater.* **2015**, *27*, 1153-1156; b) M. Dasog, G. B. De los Reyes, L. V. Titova, F. A. Hegmann, J. G. C. Veinot, *ACS Nano* **2014**, *8*, 9636-9648; c) M. Dasog, Z. Yang, S. Regli, T. M. Atkins, A. Faramus, M. P. Singh, E. Muthuswamy, S. M. Kauzlarich, R. D. Tilley, J. G. C. Veinot, *ACS Nano* **2013**, *7*, 2676-2685.

[29] J. R. Lakowicz, *Principles of Fluorescence Spectroscopy*, Springer-Verlag, New York, **2008**.

[30] Analytical Methods Committee, *Analyst, Vol. 112*, **1987**, pp. 199-204.

[31] I. Fontana, A. Lauria, G. Spinolo, *Phys. Status Solidi B* **2007**, *244*, 4669-4677.

[32] A. Sillen, Y. Engelborghs, *Photochem. Photobiol.* **1998**, *67*, 475-486.

[33] D. R. Lide, H. V. Kehiaian, *CRC Handbook of Thermophysical and Thermochemical Data*, CRC Press, Boca Raton, **1994**.

[34] A. Arrigo, R. Mazzaro, F. Romano, G. Bergamini, P. Ceroni, *Chem. Mater.* **2016**, *28*, 6664-6671.

[35] *CRC Handbook of Chemistry and Physics*, 92nd ed., (Ed: W.M. Haynes), CRC Press, Boca Raton, **2011**.

[36] R. G. Pearson, *J. Am. Chem. Soc.* **1963**, *85*, 3533–3539.

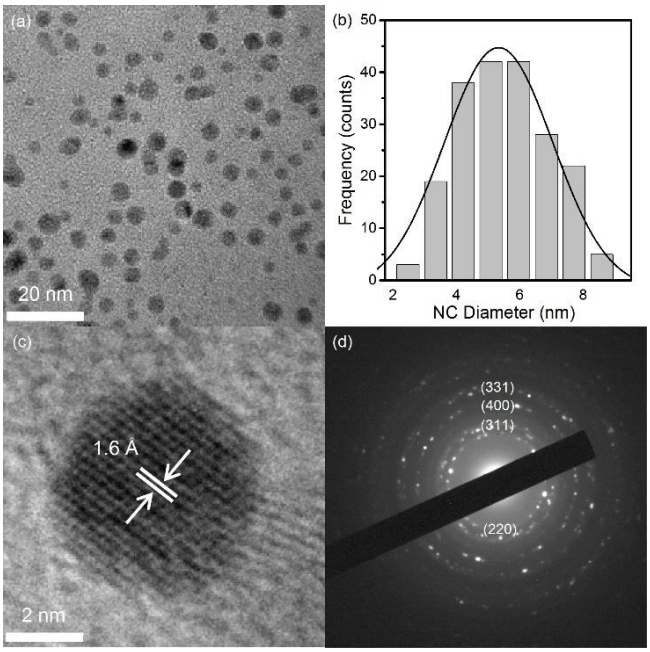

Figure 1. (a) Representative TEM image of amine-terminated Si NCs, and (b) histogram of Si NC diameters with a curve fitted to the data using a using a Gaussian model. (c) HR-TEM image of an individual Si NC, and (d) selected area diffraction pattern of the NCs.

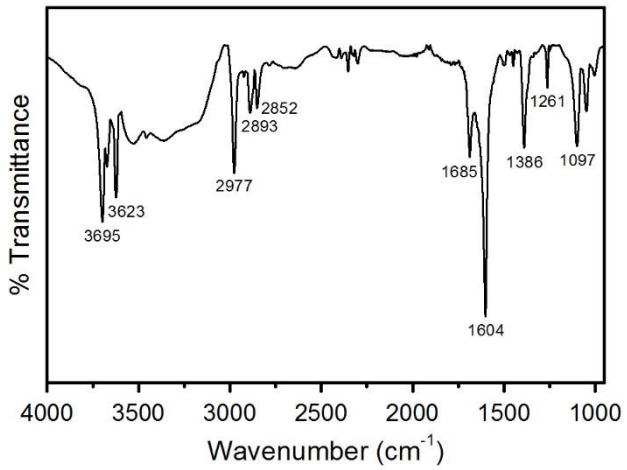

Figure 2. FTIR spectrum of amine-terminated Si NCs.

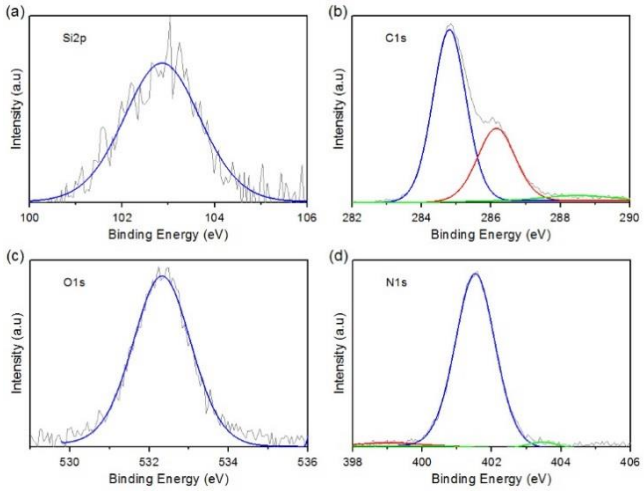

Figure 3. XPS spectra of the amine-terminated Si NCs.

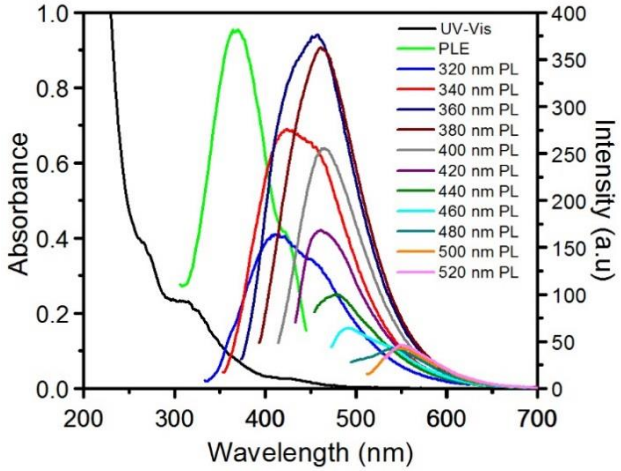

Figure 4. UV-Vis absorption, PLE and PL spectra of the Si NCs recorded at different excitation wavelengths.

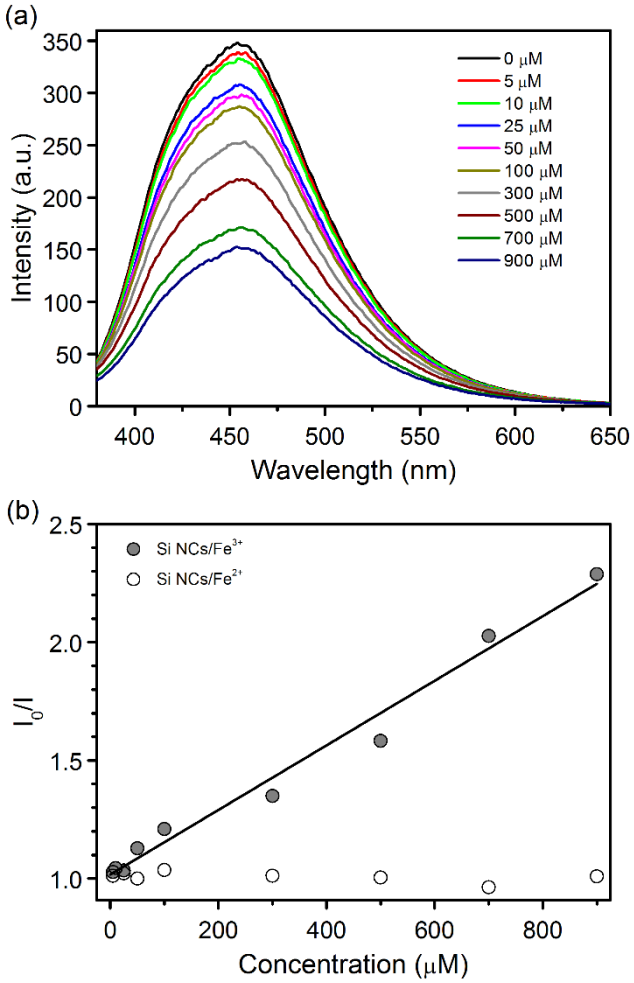

Figure 5. (a) PL spectra of Si NCs recorded at a series of Fe^{3+} concentrations, as indicated. (b) Stern-Volmer plot of I0/I vs. Fe^{3+} (grey circles) and Fe^{2+} (open circles) concentration.

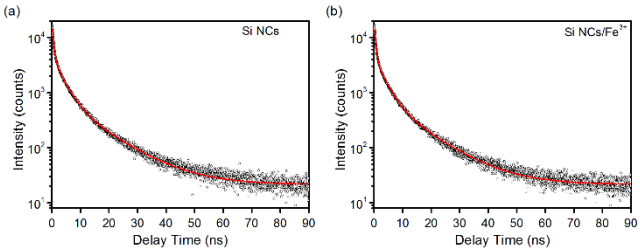

Figure 6. Nanosecond intensity transients of (a) Si NCs in pure water, and (b) Si NCs in the presence of 50 μM Fe^{3+}.

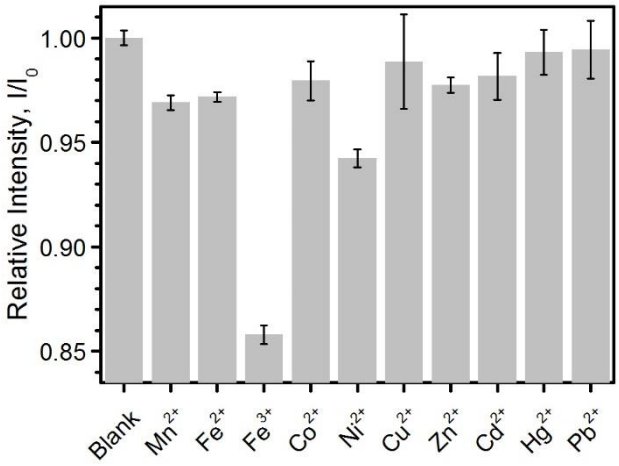

Figure 7. Relative luminescence intensity (I/I0) of the Si NCs following exposure to 50 μM of the metal ions indicated.